Structure of the Shiga-like Toxin I B-Pentamer Complexed with an Analogue of Its Receptor Gb_3[†,‡]

Hong Ling,[§] Amechand Boodhoo,[||] Bart Hazes,[||] Maxwell D. Cummings,[§,⊥] Glen D. Armstrong,[||] James L. Brunton,[@] and Randy J. Read*[,§,||]

Department of Biochemistry, University of Alberta, Edmonton, Alberta T6G 2H7, Canada, Department of Medical Microbiology & Immunology, University of Alberta, Edmonton, Alberta T6G 2H7, Canada, and Departments of Medicine and Microbiology, University of Toronto, Ontario M5G 2C4, Canada

Received July 24, 1997; Revised Manuscript Received November 25, 1997

ABSTRACT: Shiga-like toxin I (SLT-I) is a virulence factor of *Escherichia coli* strains that cause disease in humans. Like other members of the Shiga toxin family, it consists of an enzymatic (A) subunit and five copies of a binding subunit (the B-pentamer). The B-pentamer binds to a specific glycolipid, globotriaosylceramide (Gb_3), on the surface of target cells and thereby plays a crucial role in the entry of the toxin. Here we present the crystal structure at 2.8 Å resolution of the SLT-I B-pentamer complexed with an analogue of the Gb_3 trisaccharide. The structure reveals a surprising density of binding sites, with three trisaccharide molecules bound to each B-subunit monomer of 69 residues. All 15 trisaccharides bind to one side of the B-pentamer, providing further evidence that this side faces the cell membrane. The structural model is consistent with data from site-directed mutagenesis and binding of carbohydrate analogues, and allows the rational design of therapeutic Gb_3 analogues that block the attachment of toxin to cells.

Shiga toxin and Shiga-like toxins (SLTs[1] or verotoxins) form a family of structurally and functionally related proteins that are associated with disease in humans and animals (*1*). Shiga toxin is produced by *Shigella dysenteriae*, whereas SLTs are produced by certain enterohemorrhagic *Escherichia coli* (EHEC). The *E. coli* toxins can be further divided into Shiga-like toxins I and II (SLT-I and SLT-II) and the Shiga-like toxin II edema variant (SLT-IIe or pig edema toxin).

EHEC infection is sometimes called "hamburger disease" because it often results from eating contaminated hamburger meat. Infection with *S. dysenteriae* or EHEC in humans results initially in diarrhea. Frequently, disease due to EHEC progresses to hemorrhagic colitis (*2, 3*), which, in about 10% of the cases, progresses further to the hemolytic uremic syndrome or to the related syndrome of thrombotic thrombocytopenic purpura (*4, 5*). The hemolytic uremic syndrome, which is a direct result of SLT-induced kidney damage, is the major cause of acute renal failure in children (*6*). The mortality rate is 2.7−5.7% for children with the syndrome (*7*). Since clinical results suggest that conventional antimicrobial therapies are not useful and may even be counterproductive (*8, 9*), there is a great need to develop new therapies to treat the diseases caused by *S. dysenteriae* and EHEC strains.

The SLTs are AB toxins; they have an enzymatic (A) component and a cell-binding (B) component (*10*−*12*). For SLTs, the A-component is an *N*-glycosidase that inhibits protein synthesis by specifically removing the adenine base at position 4324 of 28S rRNA (*13*). The A-subunit is situated on one face of the B-component, which is a pentamer of identical subunits, and its C-terminus is anchored in a central pore of the B-pentamer (*14*).

The B-pentamer is responsible for toxin attachment to the host cell. In the absence of the A-subunit, the B-subunits still form pentamers that are functionally equivalent to the holotoxin in their binding to cell surface glycolipids (*15*). The functional receptor of the SLT family is the glycolipid globotriaosylceramide [Gb_3, αGal(1−4)βGal(1−4)βGlc-ceramide] (*16*−*18*). The importance of the B-pentamer−Gb_3 interaction is clearly illustrated by the fact that all cells that are susceptible to SLTs express Gb_3 on their cell surfaces, whereas cells that do not express Gb_3 are resistant to the toxins (*19*). In addition, it has been found that in vivo toxicity is correlated with binding affinity. Therefore,

† The research in R.J.R.'s laboratory was supported by Grant MT 11000 from the Medical Research Council of Canada (MRC) and in part by an International Research Scholarship from the Howard Hughes Medical Institute. R.J.R. is a Senior Scholar of the Alberta Heritage Foundation for Medical Research. B.H. was supported by a postdoctoral fellowship from the MRC. G.D.A.'s work was supported by an NCE grant from the Canadian Bacterial Diseases Network. The research in J.L.B.'s Laboratory was supported by MRC Grants PG11123 and MT13071.

‡ The coordinates and structure factors have been deposited in the Brookhaven Protein Data Bank (identifier 1BOS).

* To whom correspondence should be addressed. Telephone: 403-492-4305. Fax: 403-492-7521. E-mail: Randy.Read@UAlberta.CA.

§ Department of Biochemistry, University of Alberta.

|| Department of Medical Microbiology & Immunology, University of Alberta.

⊥ Present address: Computational Chemistry/Molecular Modeling, SmithKline Beecham Pharmaceuticals, 709 Swedeland Rd., King of Prussia, PA 19406.

@ University of Toronto.

[1] Abbreviations: SLTs, Shiga-like toxins; SLT-I, Shiga-like toxin I; SLT-II, Shiga-like toxin II; SHT, Shiga toxin; Gb_3, globotriaosylceramide; Gb_4, globotetraosylceramide; Gal, galactose; Glc, glucose; Pk-MCO, αGal(1−4)βGal(1−4)βGlc(1−8) methoxycarbonyloctyl; Pk, αGal(1−4)βGal(1−4)βGlc; OB fold, oligomer binding fold; rms, root-mean-square.

S0006-2960(97)01806-0 CCC: $15.00
Published on Web 02/03/1998

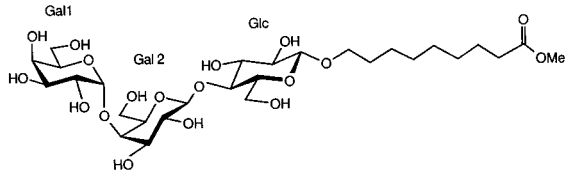

FIGURE 1: Cell surface receptor Gb_3 analogue 8-(methoxycarbonyl)-octyl trisaccharide, or Pk-MCO. The Pk trisaccharide terminus is the same as the carbohydrate portion of the glycolipid Gb_3 [αGal-(1−4)βGal(1−4)βGlc(1−1)-ceramide], which is recognized by the B-pentamer of SLT-I.

binding to the cell surface is a crucial initial step in the cytotoxicity of SLTs, and consequently, blocking toxin binding is an elegant way to protect host cells from attack by the toxins. Glycolipid analogues that have the same trisaccharide component as Gb_3 are being tested as potential agents for preventing hemolytic uremic syndrome in children with O157:H7 colitis (*20, 21*).

Shiga toxin and Shiga-like toxin I are the most similar members in the family. They only differ in one residue (Ser45 vs Thr45) in their A-subunits (*22*) and have identical B-subunits (*23*). Crystal structures of the SLT-I B-pentamer (*24*) and of the Shiga holotoxin (*14*) have been determined previously, but neither structure contained bound receptor. However, two possible receptor binding sites have been modeled (*25, 26*), including one predicted on the basis of conserved surface residues within the family (*24*). We report here the crystal structure of the SLT-I B-pentamer complexed with a Gb_3 analogue. The structure reveals the existence of not one but three Gb_3-binding sites per B-subunit, one of which corresponds to the predicted site. Our structural results provide the first direct observation of the detailed interactions between the toxin and its receptor that mediate target cell recognition.

METHODS

The SLT-I B-subunit was purified as previously described (*27*). Crystals of the B-pentamer complexed with the Gb_3 trisaccharide analogue (Figure 1) were grown at room temperature by vapor diffusion in a hanging drop. The starting drop contained 3 μL of protein solution (4 mg/mL protein, 50 mM Pk-MCO) and 3 μL of a well solution [5−19% $(NH_4)_2SO_4$, 50 mM sodium/potassium phosphate, and 2% propanol at pH 6.0]. The typical size of crystals used in data collection was about $0.3 \times 0.2 \times 0.1$ mm^3. Diffraction data were collected to 2.73 Å resolution at room temperature using a Siemens multiwire area detector and were processed using the program XENGEN 2.0 (*28*). Ultimately, the data beyond 2.8 Å resolution were not used, as discussed below. The data set used in the final refinement has a completeness of 81.6% to 2.80 Å resolution with 57.3% completeness in the highest-resolution shell (2.98−2.80 Å). Although the data beyond 3.6 Å resolution are rather weak, they did contribute favorably to the quality of the electron density maps (see Results and Discussion).

The structure of the complex was solved by molecular replacement using a preliminary data set to about 4 Å resolution. It emerged during molecular replacement calculations that there are four pentamers in the asymmetric unit, although there is sufficient volume for five. The AMORE package (*29, 30*) was used for the rotation function, whereas BRUTE (*31*) was used to refine the initial orientations and to find the positions of pentamers in the unit cell.

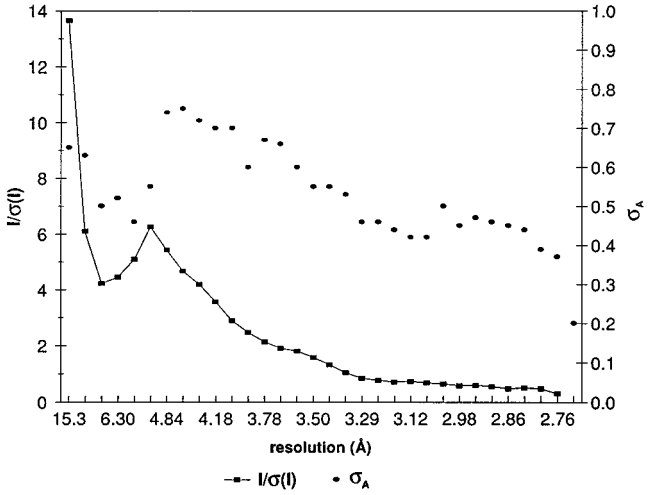

FIGURE 2: Average intensities and σ_A values as a function of resolution. σ_A values were estimated with the program SIGMAA (*34*) on the basis of the observed amplitudes and amplitudes calculated from the molecular replacement model after rigid body refinement at 3.6 Å resolution.

Two search models were tested: (i) the native SLT-I B-pentamer, which has a 5-fold screw symmetry (*24*), and (ii) a symmetric B-pentamer, which was constructed from the native model by removing the translation component along the 5-fold axis while preserving the intermonomer interaction (*32*). The correlation coefficient of the highest cross-rotation peak for the native model is 0.20, while this value is 0.32 for the symmetric one. As the symmetric search model gave significantly stronger peaks, it was used for all further steps. In the cross-rotation function, the 5-fold symmetry was represented by five related peaks with similar heights. The highest peak of the cross-rotation function was selected, and in BRUTE, two independent positions for the pentamer were found. Apparently, there are two pentamers with a nearly identical orientation in the asymmetric unit. This is supported by a low-resolution (21−10 Å) native Patterson map, which shows a non-origin peak (30% of the origin peak) relating these two pentamers. In subsequent steps, the second and third independent solutions from the cross-rotation function were positioned with BRUTE, while keeping the previously positioned pentamers fixed. The final molecular replacement solution gave an *R* factor of 44% (10−4 Å).

The model was refined with X-PLOR (*33*). During an initial rigid body refinement, each pentamer in the asymmetric unit was treated as a rigid group. Then further refinement was carried out by treating each of the 20 monomers in the asymmetric unit as a rigid body, resulting in an *R* factor of 39% (10−4 Å). The remainder of the refinement was divided into two stages. First, a strict 20-fold noncrystallographic symmetry (NCS) was imposed in refinement using only the data in the resolution range of 10−3.6 Å. At this point, it was discovered, using the program SIGMAA (*34*), that there was a significant correlation between the structure factors calculated from the rigid body-refined model and the data up to a resolution of 2.8 Å (Figure 2). Further refinement was therefore carried out using all data from 10 to 2.8 Å, and the strict NCS constraint was replaced by an NCS restraint with a weight of 300 kcal mol^{-1} Å^{-2}. At this point, we selected a set of cross-validation reflections to monitor all further refinement steps (*35*). A slow-cooling molecular dynamics simulation was carried out

Table 1: Crystallographic Data

space group	$P2_12_12_1$
unit cell (Å)	$a = 127.5$, $b = 97.7$, $c = 164.2$
number of reflections	41 759 (21−2.8 Å)
number of measurements	113 473
R_{merge}[a] (%)	
overall	14.1
highest-resolution shell	35.5 (2.98−2.80 Å)
completeness (%)	
overall	81.6
highest-resolution shell	57.3 (2.98−2.80 Å)
model	
protein	10 800 non-H atoms
carbohydrate	1622 non-H atoms
solvent	345 water molecules
average *B* factor (Å^2)	
protein	18.7
carbohydrate	31.1
solvent	20.7
R factor (%)	17.0 (21−2.8 Å)
R_{free} (%)	22.5 (5% of all data)
rmsd bond length (Å)	0.015
rmsd bond angle (deg)	2.6
rmsd *B* across bonds (Å^2)	2.7
rmsd *B* across angles (Å^2)	5.0

[a] $R_{merge} = \sum|F_i - \langle F_i\rangle|/\sum|F_i|$.

to remove model bias that might have been introduced during the previous refinement. The presence of 20-fold NCS in our crystal will reduce the difference between *R* and R_{free} because correlations between NCS-related reflections will cause overfitting to propagate to a certain extent into the cross-validation data. Nonetheless, numerical experiments by Kleywegt and Brünger (*36*) indicate that R_{free} is still a useful indicator of the validity of a refinement protocol.

The model was analyzed and adjusted at different stages using the program O (*37*). Prior to model building, the electron density maps were improved greatly by 20-fold averaging and solvent flattening with the DEMON package (*38*). The molecular envelope for averaging was created from the atomic model, using an atomic radius of 4 Å. In the initial stage, this resulted in envelopes that did not accommodate the Pk-MCO molecules, since they were not yet part of the model. Nevertheless, the density for the Pk-MCO molecules showed up clearly after averaging in a map computed with $m(2|F_o| - |F_{ave}|)\exp(i\alpha_{ave})$ coefficients. The figure of merit, *m*, is a Sim weight (*39*) with the parameter $\sum_Q$ computed by the method of Bricogne (*40*). Evidently, the 20-fold NCS averaging is so powerful in improving the phases that the Pk-MCO molecules showed up although they were in the flattened part of the map. As a test, we have also carried out averaging with envelopes generated using an atomic radius of 8 Å. In this case, at least part of the volume containing Pk-MCO molecules is no longer flattened. However, the enlargement of the envelope decreased the efficiency of the density modification to the extent that the final results were inferior to that of 4 Å radius envelopes. After including Pk-MCO molecules in the model, averaging was still carried out between the 20 NCS-related protein monomers, but the Pk-MCO molecules were put in an unflattened ("1-fold averaged") region of the map. This procedure ensures that each Pk-MCO binding site has unbiased density, and the density cannot be an artifact of averaging. Because crystal packing seems to have more effect on the conformation of the carbohydrate than on that of the protein, a relatively weak NCS restraint of 10 kcal mol^{-1} Å^{-2} was applied to the carbohydrate during the refinement. Repeated cycles of refinement and model building were carried out until refinement converged. At this stage, individual temperature factors (*B*) were refined with a restraint of 1.0 Å^2 for NCS-related atoms and tight restraints of 0.25 and 0.5 Å^2 for bonded main chain and side chain atoms, respectively. The validity of refining *B* values was supported by the free *R* factor (*35*), which dropped from 27.2 to 24.6% (10−2.8 Å). After the *B* value refinement, water molecules were selected from peaks above 4σ in a map computed with coefficients $m[|F_o|\exp(i\alpha_{ave}) - |F_c|\exp(i\alpha_c)]$, with each accepted water molecule making at least one hydrogen bond (<3.2 Å) to the protein or sugar. After further refinement, only the water molecules with *B* factors below 40 Å^2 and with a nice spherical density were kept in the model. When X-PLOR version 3.843 was released, a bulk solvent model was created and a final cycle of refinement, including bulk solvent correction (*41*), was carried out using all data from 21 to 2.8 Å. The crystallographic data are presented in Table 1.

RESULTS AND DISCUSSION

Crystallographic Data. The crystals of the SLT-I/Pk-MCO complex were obtained by cocrystallization of the B-pentamer with the Gb_3 trisaccharide analogue as described in Methods. Soaking experiments were not successful, and an a posteriori analysis of the Gb_3-binding sites indicates that Pk-MCO binding is indeed incompatible with the lattice contacts in the native crystal. The crystals of the complex have the space group $P2_12_12_1$, with the following unit cell dimensions: $a = 127.5$ Å, $b = 97.7$ Å, and $c = 164.2$ Å; there are four pentamers in the asymmetric unit. Unfortunately, the crystals diffract weakly, and although data were collected from several crystals, the I/σ_I ratio always dropped below 2 at approximately 3.6 Å resolution (Figure 2). A resolution cutoff at 3.6 Å did not hinder the molecular replacement procedure, but the initial electron density maps were of poor quality. However, the presence of 20-fold noncrystallographic symmetry (NCS) and high solvent content ($V_m = 3.25$, 62% solvent) makes electron density averaging and solvent flattening very powerful. These techniques allowed us to obtain high-quality electron density maps despite weak diffraction data. To determine a more rational resolution cutoff value, the program SIGMAA (*34*) was used to compare the observed structure factors with those calculated from the initial molecular replacement model after rigid body refinement at 3.6 Å resolution. Figure 2 shows that the σ_A coefficients are significantly above zero up to 2.8 Å resolution; i.e., the extremely weak higher-resolution data still contain useful information. On the basis of this analysis, the structure has been refined using all data to 2.8 Å resolution. The final model includes four B-pentamers, 60 Pk-MCO sugars, and 345 water molecules (Table 1), as well as a contribution for bulk solvent (*41*). The final *R* factor and R_{free} are 17.0 and 22.5%, respectively (see Table 1). A Ramachandran plot is presented in Figure 3.

Overall Structure. The four B-pentamers in the asymmetric unit are very similar, and the rms deviations for the main chain atoms are within 0.2 Å between the pentamers and 0.1 Å between the monomers. The Ramachandran plot also clearly shows that the main chain conformations are virtually identical in all 20 B-subunits (Figure 3). In view of the high structural similarity, we will limit our discussion to one of the four pentamers.

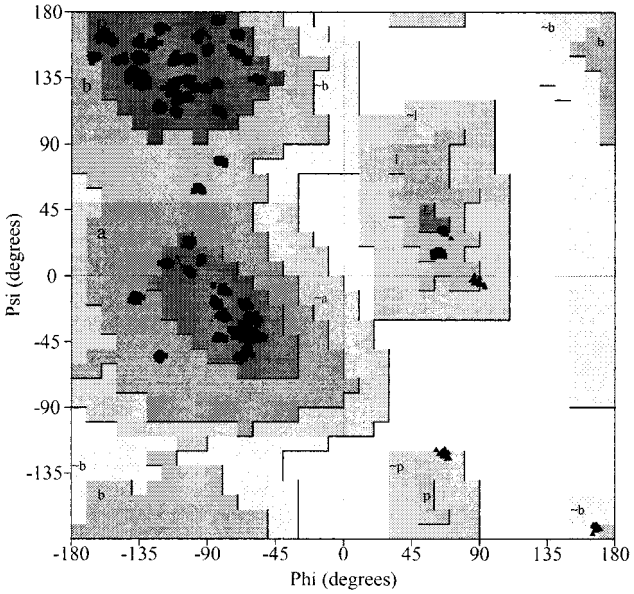

FIGURE 3: Ramachandran plot of the four SLT-I B-pentamers in the asymmetric unit. Ninety percent of the residues are located within the most favored regions (A, B, and L); 10% of the residues are located in the additional regions (a, b, l, and p), and none are in disallowed regions. Filled triangles and squares represent glycine and non-glycine residues, respectively. Clusters of points correspond to the 20 copies of each residue, indicating that conformations of the monomers are very similar. This diagram was prepared using the program PROCHECK (*64*).

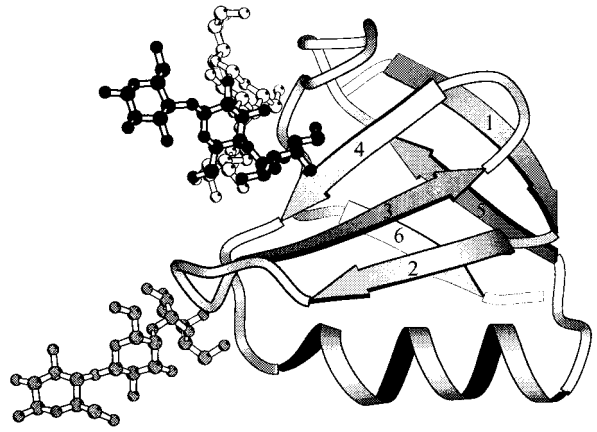

FIGURE 4: Schematic diagram of the OB (oligomer binding) fold: one SLT-I B-subunit with three Gb_3 trisaccharides. Six antiparallel β-strands (numbered arrows) form a closed β-barrel, capped by an α-helix located between the fourth and fifth strands. Three Pk-MCO molecules bind to one side of the β-barrel and are black at site 1, white at site 2, and gray at site 3 [Figure made with MOLSCRIPT (*65*)].

The B-subunit monomer contains 69 residues (*12*) and has a typical oligomer-binding (OB) fold that consists of a six-stranded antiparallel β-barrel capped by an α-helix (Figure 4). The three-stranded β-sheets of neighboring monomers interact with each other across the subunit interface to form six-stranded sheets, whereas the five helixes line a central pore along the 5-fold axis (Figure 5a). The OB fold has been found in several proteins that bind an oligosaccharide or an oligonucleotide, and all these proteins have a single binding site in a structurally conserved location (*42*). Our structure determination, however, reveals three binding sites in each SLT-1 B-subunit, i.e., 15 binding sites per B-pentamer. These three distinct binding sites are referred to as sites 1−3 (Figure 5a). Site 1 corresponds to the previously predicted binding site (*24*), whereas site 2 is topologically equivalent to the binding sites found in the other OB fold proteins.

Structural Comparisons. The SLT-I/Pk-MCO complex has more exact 5-fold symmetry than the native SLT-I B-pentamer, which has a screw component along its 5-fold axis (*24*). The B-pentamer of Shiga holotoxin (SHT), which is identical in sequence to the SLT-I B-pentamer, also has pure 5-fold symmetry (*14*) and is very similar to our SLT-I/Pk-MCO complex structure. The rms deviation between the B-pentamers of SLT-I/Pk-MCO and SHT is 0.5 Å for main chain atoms. The main chain rms deviation between the SLT-I/Pk-MCO monomer and the native SLT-I monomer is 0.3 Å. However, when the entire B-pentamers are compared, the rms deviation becomes 1.6 Å, reflecting the presence of a 5-fold screw axis in the native structure. This difference between the B-pentamers of native and complexed SLT-I is also indicated by the molecular replacement results, as the 5-fold symmetric model gives significantly higher correlation coefficients than the native model. The structural comparisons indicate that the individual B-subunits do not undergo significant conformational changes upon Pk-MCO binding; i.e., the OB fold is relatively rigid and the sugar-binding sites appear to be preformed before sugar binding. Most of the side chains also adopt a similar conformation in both native and complex structures. However, the side chain of tryptophan 34 changes its conformation upon Pk-MCO binding (Figure 6).

Tryptophan 34 is fully exposed to the solvent on the Gb_3-binding surface of the B-pentamer. It is located on the N-terminal end of the α-helix, and five symmetry-related tryptophan side chains surround the central pore of the pentamer (Figure 6). In the native SLT-I structure, one of the tryptophan side chains projects vertically out of the binding surface, while the other four tryptophans point toward the 5-fold axis so that their hydrophobic indole rings interact favorably with each other. However, this interaction requires a screw component to be present along the 5-fold axis in order to prevent a steric conflict between indole rings. Indeed, in the Shiga holotoxin, which has pure 5-fold symmetry, the tryptophan side chains do not adopt the same conformation since that would cause the steric conflict. Instead, the tryptophan side chains appear to be disordered (*14*). In contrast, the five tryptophan rings are well defined in the SLT-I/Pk-MCO complex structure, but in this case, the indole rings point away from the central pore (Figure 7, Figure 6). Interestingly, the tryptophan in the complex adopts an uncommon side chain conformation ($\chi_1 = -74°$, $\chi_2 = 10°$). This observation suggests that Pk-MCO binding stabilizes the uncommon tryptophan conformation.

Pk-MCO Trisaccharide Binding. In our cocrystallization experiments, we have used the more soluble Gb_3 analogue αGal(1−4)βGal(1−4)βGlc 8-(methoxycarbonyl)octyl (Pk-MCO, Figure 1). This analogue has only a single alkyl chain, which is also shorter than the ones in Gb_3. However, its trisaccharide moiety (Pk), which is the actual part that is recognized by SLT-I, is identical with that of Gb_3. In the remainder of this paper, we will generally use Pk to refer to this trisaccharide and Gal1, Gal2, and Glc to refer to the three sugar residues αGal, βGal, and βGlc.

All Gb_3-binding sites are located on the same flat face of the B-pentamer (Figure 8, Figure 5a), opposite the A-subunit (Figure 5b). There are no interactions between the binding

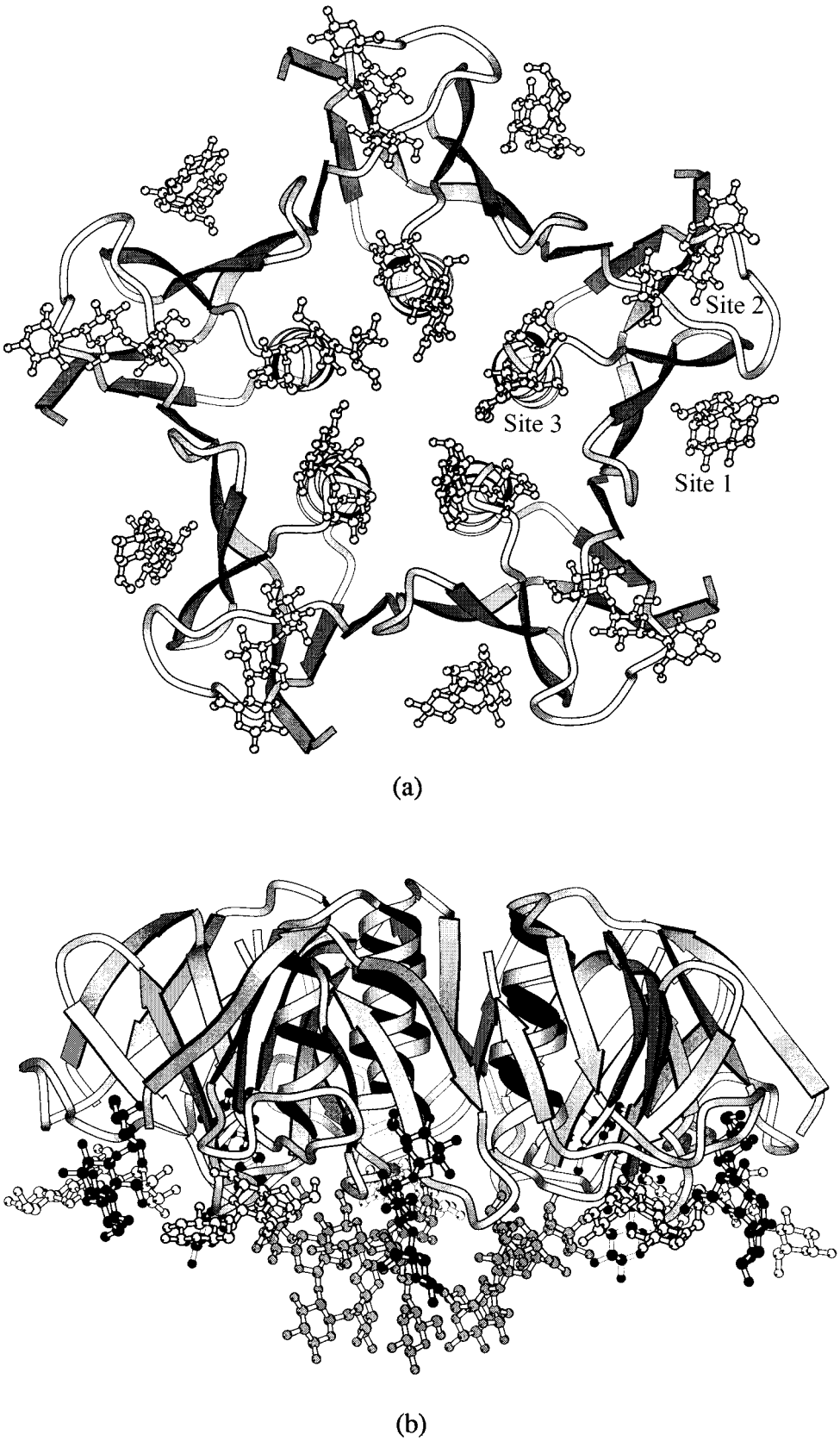

FIGURE 5: Two orthogonal views of the SLT-I B-pentamer bound to the Pk-MCO trisaccharides. (a) View along the 5-fold axis. The surface toward the viewer is the sugar binding surface, which corresponds to the bottom surface in the view shown in panel b. Binding site 1 (black in panel b) is located in the groove close to an adjacent B-subunit of the pentamer, and the sugar moieties contact strands β3 and β4. At binding site 2, the trisaccharide chain (white in panel b) lies nearly parallel to the surface and contacts the loops β2−β3 (from a neighboring monomer), β4−α, and β5−β6. At binding site 3, the sugars (gray in panel b) are at the N-terminal end of the helix of each monomer, located around the central pore of the pentamer and interacting with loops β4−α and β2−β3 (from a neighboring monomer). In the SHT holotoxin structure (*14*), the A-subunit is located on the face opposite the binding sites (top side in panel b) [figures made with MOLSCRIPT (*65*)].

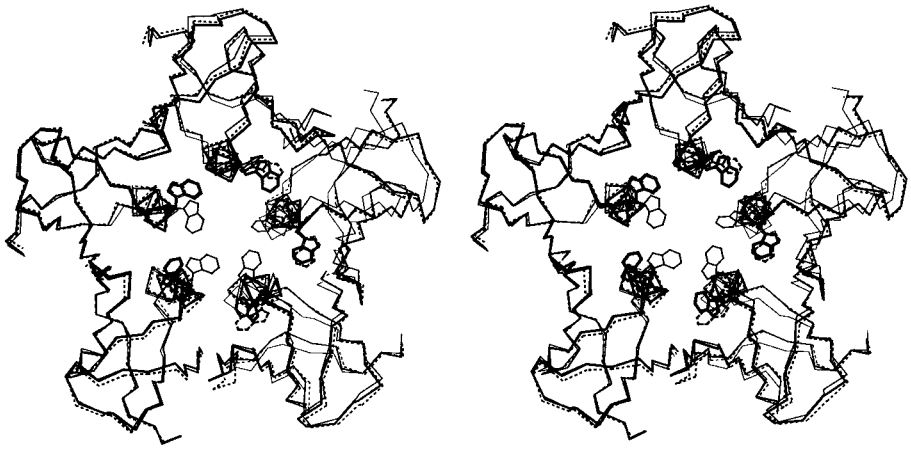

FIGURE 6: Stereodiagram of superimposed Cα backbones of B-subunits from SHT (dashed line), native SLT-I (thin line), and the SLT-I complexed with Pk-MCO (thick line), viewed along the 5-fold axis. The corresponding Trp34 residues are shown as well. The side chains of Trp34 of SHT and the SLT-I complex take similar orientations, in contrast to those in the native SLT-I B-pentamer [figure made with MOLSCRIPT (*65*)].

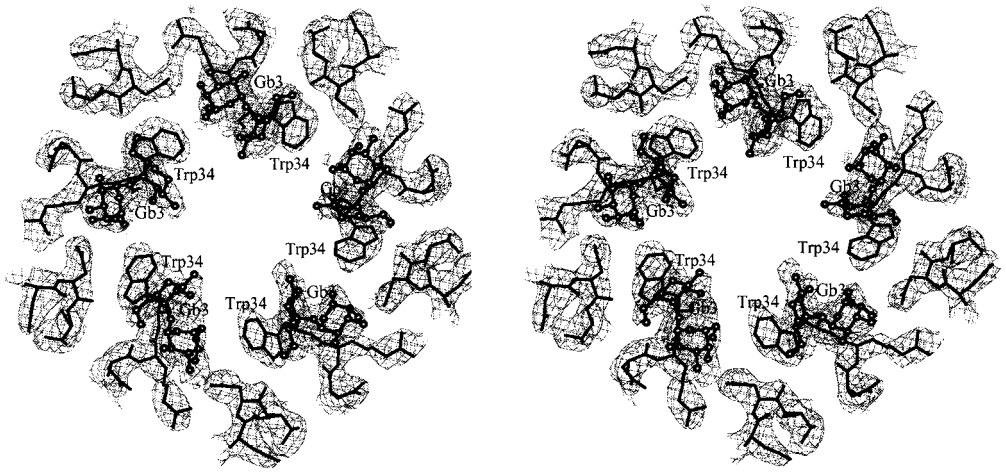

FIGURE 7: Stereoview of the final electron density in the vicinity of Trp34, after averaging over only the protein region. The map is computed using data from 21 to 2.8 Å resolution with coefficients $m(2|F_o| - |F_{ave}|) \exp(i\alpha_{ave})$. The map is contoured at 1.0 times the rms electron density. For clarity, only contours within 1.8 Å of an atom in the figure are shown. The view is the same as in Figure 5a. The five tryptophan rings all point away from the central pore, and their electron density is very well defined. The partially shown Pk-MCO trisaccharide molecules (labeled as Gb_3) are located between the indole rings in site 3 [figure made with BOBSCRIPT (*66*)].

sites, which suggests that the Pk trisaccharides bind independently of one another. Two of the binding sites (sites 2 and 3) are constructed by residues from two different monomers and thus require the pentameric assembly of the B-pentamer (Figure 9b,c).

The final averaged electron density map defines the sugar residues unambiguously at most binding sites (Figure 10). In some sites, there is even density for part of the alkyl chain, although that part has not been modeled yet (Figure 10a,b). There is, however, variation in the quality of the electron density, both between different sites and between equivalent sites related by NCS. The variation in the quality of electron density suggests that Pk-MCO binds to these sites with different affinities. For the different binding sites, this probably reflects the actual different interactions between the isolated trisaccharide and the protein. (The relative affinities could change for glycolipids constrained on a membrane surface.) For the binding sites related by NCS, the differences appear to be mainly due to crystal packing. For example, in binding site 1, the B-subunits that have better density for Pk-MCO are generally near another B-pentamer. Conversely, B-subunits in which binding site 1 is fully exposed to the solvent have much weaker carbohydrate density. A similar variation in the quality of electron density was observed for the binding of the G_{M1} oligosaccharide to the cholera toxin B-pentamer (*43*). Table 2 summarizes how well the electron density defines the carbohydrate molecules in all 60 binding sites.

Binding Site 1. In site 1, Pk-MCO interacts with strands β3 and β4 and loops β2−β3 and β5−β6 (Figure 9a). Interestingly, the double mutant D16H/D17H has almost completely lost its Gb_3 binding activity (*44*), suggesting a potential role for Asp17. This agrees with our structural results since Asp17 accepts a hydrogen bond from the 6′-hydroxyl of Gal2 in site 1 (Table 3, Figure 9a). However, Asp16 is involved in Pk-MCO binding in site 2 (see below). Accordingly, the double mutant affects both binding sites 1 and 2, and it is therefore unclear from the mutagenesis experiment what the individual contributions of these two residues are to receptor binding. Mutation of Asp17 to asparagine has been reported to have little effect on binding (*44*); this could be accommodated, although the side chain amide group would donate a hydrogen bond to O6 of Gal2 (see Figure 9a).

The hydrophobic interactions at site 1 (Table 4) are dominated by Phe30, which stacks against the B-face of

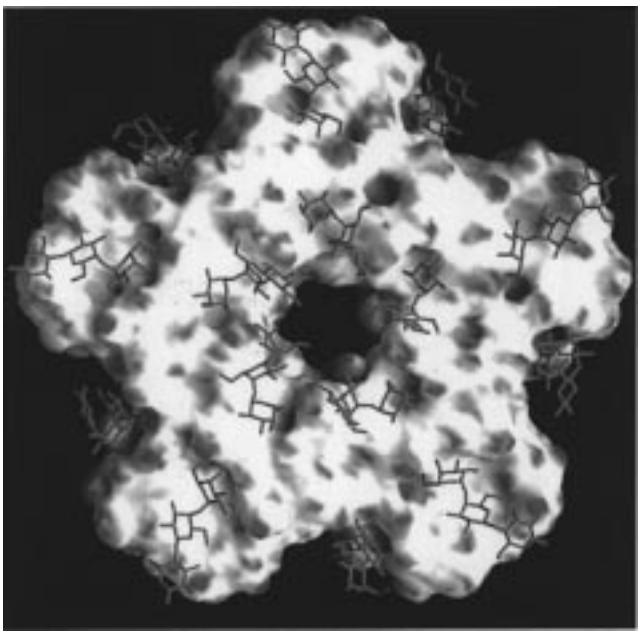

FIGURE 8: Surface curvature representation of the membrane binding surface of the B-subunits, with Pk-MCO trisaccharides arranged on top of this surface. The protein surface is colored from green (for convex surfaces) to gray (for concave surfaces), and the Gb_3 analogue is shown in purple. Binding sites 2 and 3 appear as shallow grooves, while site 1 is located in a deeper cleft [image produced using the program GRASP (*67*)].

Gal2. This stacking interaction is typical for many protein−carbohydrate interactions (*45*) and especially for the β-anomer of galactose residues (*46*). Quiocho et al. (*47*) proposed that this kind of interaction may actually confer galactose specificity. Phe30 also contacts the Pk-MCO molecule at binding site 2 (see below). The importance of Phe30 in Gb_3 binding is supported by an F30A mutant, which has a 4-fold reduction in affinity for Gb_3 in a microtiter plate assay, and 10^5-fold reduction in cytotoxicity (*48*). A recent NMR study of the SLT-I B-subunit in solution (*49*) also suggests that Gb_3 binding involves a stacking interaction between Gal2 and an aromatic group, which is likely Phe30 but could also be Trp34 in site 3, as discussed below.

A significant role for site 1 in the SLT family is also supported by mutagenesis and modeling results on SLT-IIe, which binds to Gb_4 preferentially. SLT-IIe is closely related to SLT-II, differing only by nine sequence substitutions and a deletion at the C-terminus, but SLT-II binds to Gb_3. Tyrrell et al. (*50*) constructed a series of SLT-IIe mutants by substituting residues from the SLT-II sequences and found that in the double mutant Q65E/K67Q (designated GT3) the binding preference is altered from Gb_4 to Gb_3. The GT3/Pk-MCO complex structure has also been solved, and two binding sites corresponding to sites 1 and 2 in the present complex have been revealed (H. Ling and R. J. Read, unpublished results). The two mutated residues are on the surface of the B-pentamer and are close to the terminal residue (Gal1) of Pk-MCO in site 1. This implies that SLT-IIe probably has a Gb_4 binding site at a location corresponding to site 1 in SLT-I, which is disturbed by the double mutation. A modeling experiment, described in the following paper, shows that the extra GalNAc residue of Gb_4 can be attached in a favorable conformation to the Pk-MCO molecule in site 1, while interacting with residues 65 and 67 in SLT-IIe (*51*). The crystallographic result and modeling work provide further evidence that site 1 is a conserved binding site in the SLT family.

Binding Site 2. The Pk-MCO trisaccharide in binding site 2 is oriented approximately parallel to the protein surface, which allows all three sugar residues to interact directly with the protein. This extensive interaction probably contributes to the strong density that is observed at site 2. The actual interaction with the protein is dominated by numerous hydrogen bonds made by Gal1 (Table 3). Although a stacking interaction with an aromatic side chain is typical, such an interaction is not present at this binding site. The amino acids that constitute binding site 2 are donated by loops $\beta2-\beta3$, $\beta4-\alpha$-helix, and $\beta5-\beta6$ from a neighboring subunit. The involvement of Asp16 in binding (Table 3, Figure 9b) is consistent with the results of the double histidine mutation mentioned in connection with site 1. In the same work, a D16N mutant was found to retain binding activity (*44*). This agrees with our structural results as an asparagine side chain could make the same hydrogen-bonding interaction.

A G62T mutant of the SLT-I B-subunit has been constructed, on the basis of the prediction that this would disrupt site 2 selectively. In fact, binding and toxicity are almost completely eliminated (D. Bast, L. Bannerjee, and J. L. Brunton, unpublished results). The interpretation of this result is complicated by the proximity of site 1; the side chain of Phe30 would be close to the new Thr62 side chain, and any significant shift in its position could lead to the disruption of site 1 as well (see above). Structural analysis of this mutant will be essential to determine whether this is the case.

Binding Site 3. Unlike the second binding site, the trisaccharide chain in site 3 is nearly perpendicular to the protein surface so that it has fewer contacts with the protein (Figure 9c). The amino acids involved in binding are located at the N-terminus of the α-helix and in the $\beta2-\beta3$ loop around the central pore (Figure 5). Compared to binding site 2, site 3 has fewer hydrogen bonds and is more dependent on hydrophobic interactions (Figure 9c). Only Gal1 is involved in hydrogen bonding (Table 3, Figure 9c), including a bidentate hydrogen bond from the side chain carboxylate of Asp18. Interestingly, a D18N mutant binds to Gb_4 as well as Gb_3 (*50*). Gb_4 [globotetraosylceramide, βGalNAc-(1−3)αGal(1−4)βGal(1−4)βGlc-Cer] is the preferred receptor for the Shiga-like toxin II edema variant (SLT-IIe, also called pig edema toxin), and SLT-IIe has an asparagine at position 18 (*52*). The proximity of residue 18 to the position that would be occupied by the extra GalNAc residue in Gb_4 suggests that site 3 may be a Gb_4 binding site in SLT-IIe. However, an extra GalNAc residue at site 2 would also be reasonably close to this residue (Figure 9b), so further structural work will be required to clarify the role of Asn18 in Gb_4 binding by SLT-IIe.

The hydrophobic interactions at site 3 are dominated by Trp34. As discussed earlier, the Trp34 side chain orientation differs from that in the native structure and is more exposed to solvent. In this orientation, one face of the indole ring interacts with Gal1 of a neighboring subunit, whereas the other face stacks onto the B-face of Gal2. This is similar to the stacking interaction involving Phe30 in site 1. Surprisingly, site-directed mutagenesis studies show that substitution of Trp34 with alanine does not decrease the binding affinity, but does decrease the number of Gb_3 binding sites recognized in a microtiter assay (D. Bast and J. L. Brunton, unpublished

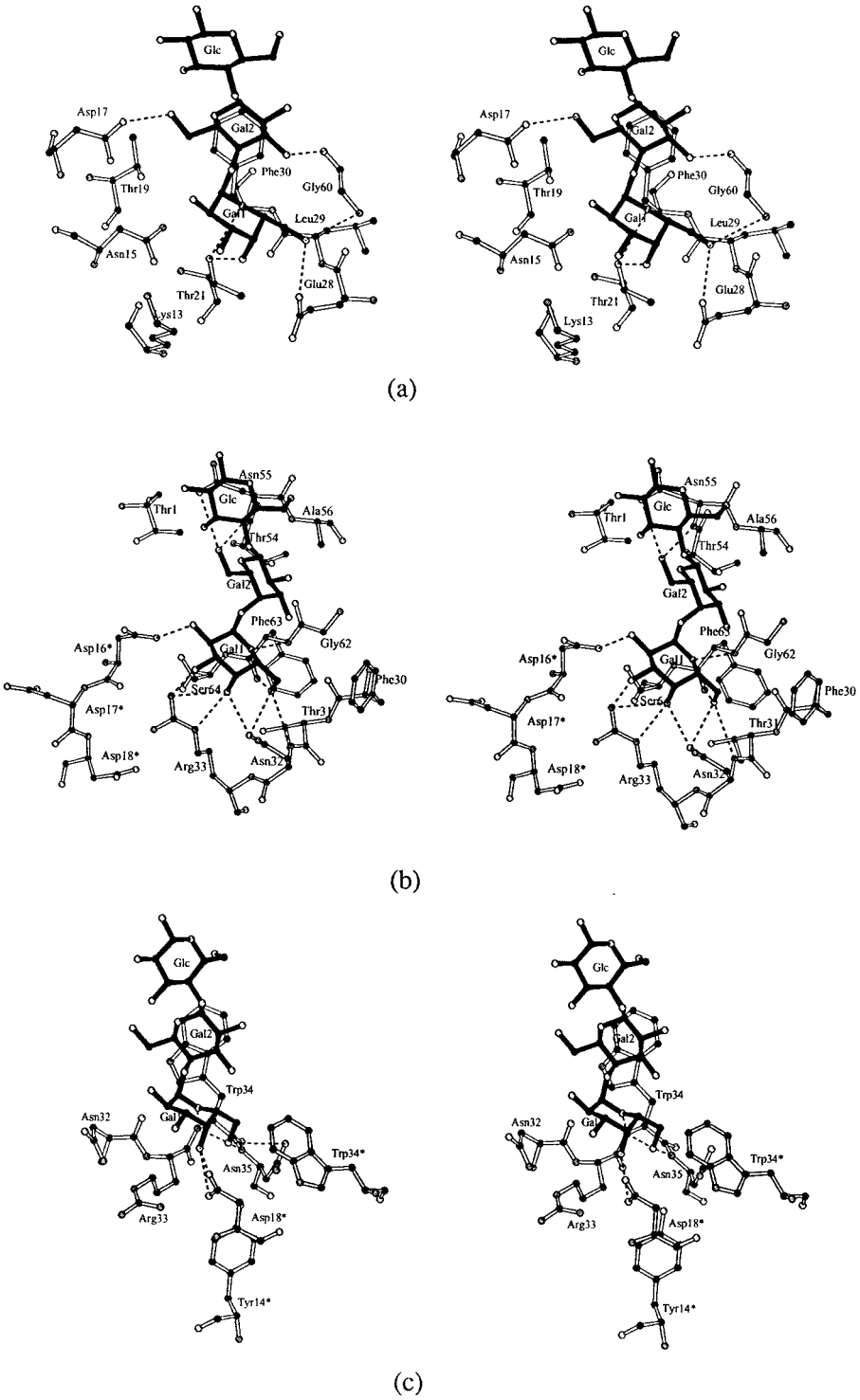

FIGURE 9: Stereodiagrams of the Gb_3 receptor-binding sites of the SLT-I B-subunit prepared using the program MOLSCRIPT (*65*). Dashed lines indicate intermolecular hydrogen bonds, and asterisks indicate amino acid residues from neighboring B-subunits of the pentamer. (a) The Pk-MCO trisaccharide at site 1. The aromatic ring of Phe30 stacks against the second galactose (Gal2) of Pk-MCO. (b) The Pk-MCO trisaccharide at site 2. (c) The Pk-MCO trisaccharide at site 3 (around the central pore of the pentamer). The indole ring of Trp34 stacks against the second galactose (Gal2) of Pk-MCO.

results). Cytotoxicity is reduced only 2−100-fold, depending on cell type, which is much less than the 10^5-fold reduction noted with the Phe30 mutation. Similar cytotoxicity results were obtained by Jemal et al. (*53*), who produced Gly and Phe substitutions at position 34.

Conformation of the Gb_3 Trisaccharide. The Gb_3 trisaccharide can adopt multiple conformations due to freedom of torsion angles in the glycosidic linkages between sugar rings. However, all 60 copies of the trisaccharide have similar conformations. The conformations observed in sites 1 and 2 do not differ significantly, and the conformations in site 3 are quite similar (Table 5). The average conformation of Pk-MCO is close to the calculated minimum energy conformation (*51*) and is also stabilized by interactions with the protein.

The orientation of the Gb_3 trisaccharide chain relative to a membrane surface depends on the conformation of the Glc−ceramide linkage when the glycolipid is inserted into

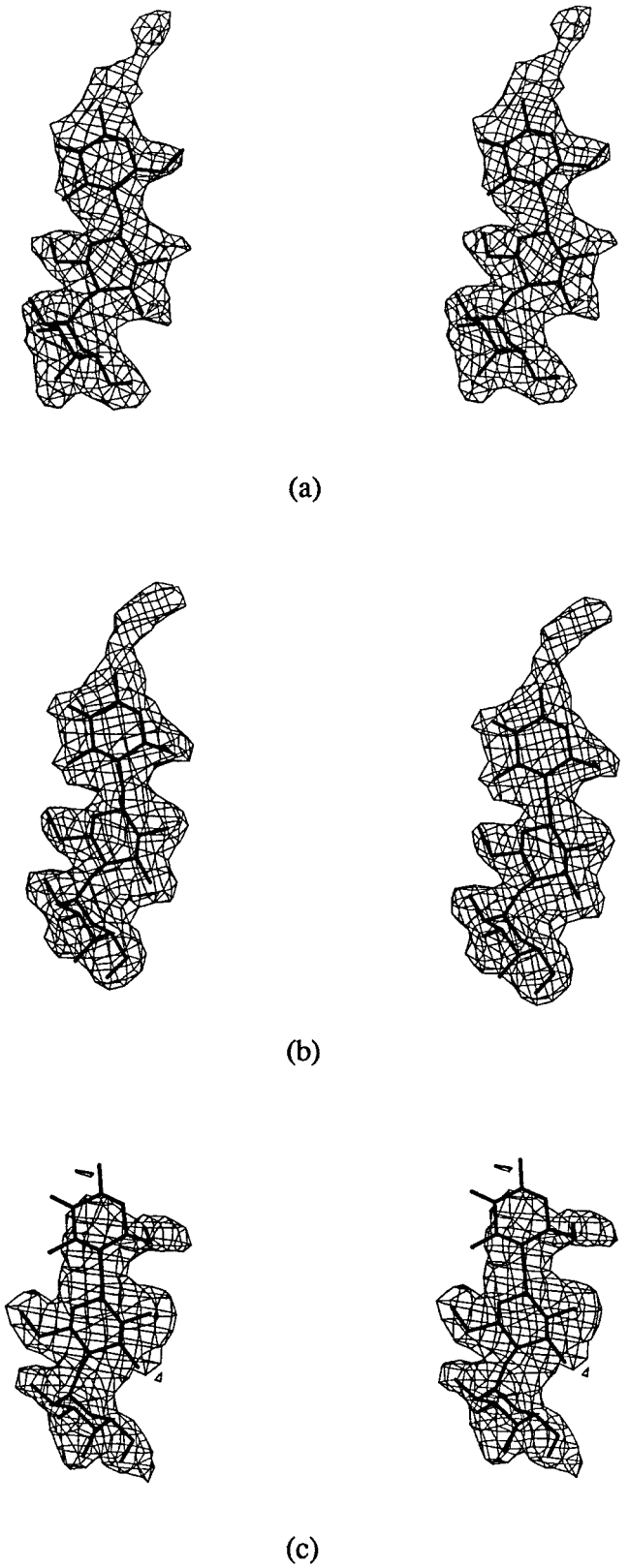

FIGURE 10: Typical electron density, from the final averaged map described in Figure 7, for Pk-MCO in its three distinct binding sites [contoured at 1.0 times the rms electron density, prepared with O (*37*)]. (a) Electron density of Pk-MCO trisaccharide bound to site 1. The quality of the density is variable, but in several cases, well-defined density covers all three sugar rings and part of the hydrophobic tails. (b) Electron density of Pk-MCO trisaccharide bound to site 2. The three sugar residues are well defined, and extra density extending from the glucose ring shows part of the hydrophobic tail. (c) At site 3, only the two galactose rings typically show well-ordered electron density.

Table 2: Pk-MCO Model Completeness over 60 Binding Sites

site	no. of sites with full Pk	no. of sites with Gal1-Gal2	no. of sites with Gal1 only
1	8	2	10
2	20	0	0
3	6	14	0

Table 3: Potential Hydrogen Bonds in Binding Sites of Pentamer 1[a]

sugar atom		protein atom		B1[b] (Å)	B2[b] (Å)	B3[b] (Å)	B4[b] (Å)	B5[b] (Å)
site 1								
Gal1	O4	Thr21	OG1	3.39	3.12	2.66	2.90	2.54
Gal1	O5	Thr21	OG1	3.29	3.11	(3.94)	3.50	(4.01)
Gal1	O6	Glu28	OE2	(3.83)	3.07	2.93	2.90	3.43
Gal1	O6	Gly60	N	3.41	(3.88)	3.30	3.17	(3.86)
Gal2	O3	Gly60	O	2.73	*c*	*c*	2.79	*c*
Gal2	O6	Asp17	OD2	2.76	*c*	*c*	2.57	*c*
site 2								
Gal1	O2	Asp16[d]	OD2	2.74	2.78	2.87	2.75	2.81
Gal1	O3	Arg33	NH2	2.99	3.00	3.13	2.95	2.91
Gal1	O4	Asn32	OD1	2.60	2.99	2.92	2.73	2.84
Gal1	O4	Arg33	NE	3.02	2.86	2.95	2.90	2.87
Gal1	O4	Arg33	NH2	3.30	3.09	3.01	3.12	3.02
Gal1	O5	Phe63	N	3.19	3.26	3.46	3.41	3.34
Gal1	O6	Asn32	N	3.19	3.18	3.31	3.30	3.36
Gal1	O6	Asn32	OD1	3.12	2.99	2.82	3.01	3.04
Gal1	O6	Phe63	O	3.04	2.73	3.06	2.69	2.74
Gal2	O6	Asn55	N	2.92	3.18	3.11	2.93	3.21
Gal2	O6	Asn55	OD1	3.30	3.23	3.28	3.41	3.38
site 3								
Gal1	O4	Asp18[d]	OD1	2.98	3.12	2.97	3.07	3.15
Gal1	O4	Asp18[d]	OD2	2.99	2.85	2.80	2.94	2.95
Gal1	O5	Trp34	N	3.12	3.14	3.07	3.22	3.31
Gal1	O6	Trp34	N	3.09	3.07	3.11	3.16	3.21
Gal1	O6	Asn35	N	2.77	2.95	2.76	3.13	2.90

[a] Donor−acceptor distances less than 3.5 Å are considered potential hydrogen bonds, and the distances of >3.5 Å are listed in parentheses. [b] Distance between potential hydrogen bonding partners in B-subunits B1−B5 of the first of the four B-pentamers. [c] Subunits B2, B3, and B5 have incomplete sugar models that lead to some missing hydrogen bonds. [d] These residues are part of a neighboring subunit.

Table 4: Hydrophobic Interactions between Sugar and Protein

site	sugar residue	protein residue
site 1	Gal1	Leu29
	Gal2	Phe30[a]
	Glc	Phe30
site 2	Gal1	Phe30, Thr31, Gly62, Ser64
	Gal2	Thr1, Thr54, Ala56, Gly62
	Glc	Asn55
site 3	Gal1	Trp34, Trp34[b]
	Gal2	Trp34[a]

[a] Aromatic stacking interaction. [b] Residue comes from the adjacent B-subunit.

the membrane. According to molecular mechanics calculations, there are three energetically favored conformers of glucose−ceramide in bilayer surface environments (*54*). Two of them (conformers 2 and 6; cf. ref *54*) have the glucose ring approximately parallel to the membrane surface, similar to the orientation of Pk-MCO in site 2 (Figure 5b, white Pk-MCO molecule), given that the membrane binding side of the B-pentamer would lie parallel to the cell membrane. The other conformer (conformer 5) has the glucose ring extended perpendicular to the surface of the cell membrane, which is consistent with the orientation of Pk-MCO in sites 1 and 3 (Figure 5b, gray and black Pk-MCO molecules). It

Table 5: Glycoside Conformations of Pk-MCO[a]

sugar linkage	angle	site 1	site 2	site 3
Gal(α1−4)Gal	φ	−47.3° (−56.4 to −31.8°)	−48.0° (−55.0 to −43.8°)	−43.6° (−51.1 to −36.2°)
	ψ	−9.4° (−17.2 to 0.6°)	−10.2° (−20.0 to 2.8°)	−1.5° (−12.3 to 6.8°)
Gal(β1−4)Glc	φ	45.0° (21.9−55.5°)	(43.6° (33.2−50.0°)	32.3° (22.8−41.0°)
	ψ	−4.3° (−33.0 to 14.3°)	2.3° (−8.2 to 7.7°)	−25.0° (−42.0 to 2.2°)

[a] φ, H1−C1−O4−C4; φ, C1−O4−C4−H4. The values listed in the table are the average angles of NCS-related Pk-MCO copies in the asymmetric unit; values in parentheses give the range of the torsion angles observed in the structure.

would therefore be possible for all observed binding sites to engage Gb_3 molecules on a target cell surface without steric conflict.

Correlation with Binding Data for Carbohydrate Analogues. Nyholm et al. (*26*) have tested the binding of various deoxy analogues of Gb_3 to several members of the Shiga toxin family. The results for SLT-I can be summarized in terms of percent binding at 100 nM compared to the control Gb_3 glycolipid: Gal2−6′-deoxy, <1%; Gal1−6′-deoxy, 3%; Gal2−2′-deoxy, 28%; Gal1−4′-deoxy, 31%; Gal1−2′-deoxy, 41%; Gal2−3′-deoxy, 68%; and Gal1−3′-deoxy, 76%. Intermolecular hydrogen bonds observed in our structure (see Table 3 and Figure 9) provide a good explanation for the importance of the exocyclic 6′-hydroxyls in both galactose residues and for the 4′-OH of Gal1. Both the 4′-OH and the 6′-OH of Gal1 form hydrogen bonds to the protein in all three binding sites, while the 6′-OH of Gal2 forms hydrogen bonds in sites 1 and 2. On the other hand, intermolecular hydrogen bonding does not explain the importance of the 2′-OH of Gal2, which is not involved in any direct interactions with the protein. Water-mediated interactions may play a role in binding, but at the current resolution, the solvent structure cannot be defined with sufficient completeness and precision. The lesser importance of the other hydroxyls is consistent with the fact that they form only single hydrogen bonds in a single binding site (site 1 for Gal2−3′-OH and site 2 for Gal1−2′- and −3′-OH).

Evaluation of Computer Modeling of Binding Interactions. Nyholm et al. (*26*) have modeled binding interactions for Gb_3 in regions corresponding to sites 1 and 2. In docking to the protein, they have started from the calculated low-energy conformation of Gb_3, which is similar both to the conformation computed by Cummings et al. (*51*) and to the conformations observed in the crystal structure. Their docking was also informed by Nyholm's previous work on allowed conformations for the Glc−Cer linkage (*54*), which limits the orientation of the glycolipid relative to the protein.

The trisaccharide docked by Nyholm et al. (*26*) at site 2 is in contact with the same general area of the protein surface as the crystallographically observed molecule, but it is in a rather different orientation. The model predicts four hydrogen bonds, none of which agrees with the eleven observed in the crystal structure (Table 3).

The modeling by Nyholm et al. (*26*) of binding at site 1 is somewhat more successful, with some of the predicted interactions agreeing with those observed in the crystal structure. The model includes the stacking interaction of the B-face of Gal2 with Phe30, which is typical of binding interactions of β-galactose residues (*46*) and which is consistent with the results from the F30A mutant (*48*). However, owing to a rotation of the trisaccharide around this point of contact, combined with small differences in carbohydrate conformation, only two of the seven predicted hydrogen bonds (Gal1 6′-OH to Glu28 and Gal2 6′-OH to Asp17) are among the six observed in the crystal structure (Table 3). (Note that Asp17 is incorrectly labeled as Asp16 in Table 1 of ref *26*, whereas it is correctly labeled in the text and figures.) Nyholm et al. (*26*) also modeled Gb_4 binding to SLT-IIe in this site, but because of the difference in orientation of the Gb_3 trisaccharide component, it differs substantially from the model presented in the following paper (*51*).

Physiological Relevance. Our structural results show that the SLT-I B-pentamer has multiple carbohydrate binding sites per monomer, instead of the single binding site found in other OB fold proteins. The larger number of binding sites may increase toxicity since it potentially allows SLT-I to bind its target cell more tightly. Still, we have to consider the possibility that host cell binding in vivo is dominated by one or two of the sites while other sites are fortuitous or serve another function.

Apart from our structural data, there are two other observations that suggest that SLT-I contains multiple binding sites per monomer. First, Scatchard analysis of Gb_3 binding to SLT-I presents a slightly concave plot, which indicates either multiple classes of sites or negative cooperativity (*55*). However, our structural results suggest that there is no interaction between binding sites, either directly or through conformational changes. Accordingly, it seems likely that the concave curve is a result of the presence of multiple binding sites. Second, the affinity of cholera toxin (CT) for G_{M1} is $\sim 10^6$ M^{-1} when G_{M1} is in solution and $\sim 10^9$ M^{-1} when G_{M1} is presented on the cell membrane (*56*−*58*). Shiga toxin also binds to whole cells with a binding constant of 10^9 M^{-1} (*59*); however, the binding constant for soluble Gb_3 is only $\sim 10^3$ M^{-1} (*55*). Only one binding site per monomer has been observed in the CT/G_{M1} structure (*43*). The presence of a larger number of binding sites on SLT-I might explain how it achieves a binding affinity for cells that is comparable to that of CT despite its much lower affinity for the soluble receptor.

The existence of multiple binding sites might also explain observations on the effect of the fatty acid moiety of Gb_3 glycolipids. Pellizzari et al. (*60*) showed that SLTs bind with different affinity to Gb_3 species that differ in the nature of the fatty acid chains, and that the tightest binding is observed for mixtures of Gb_3 species. As speculated by Nyholm et al. (*26*), the fatty acid conformation may affect the allowed conformation and the height of trisaccharide headgroups presented on the membrane surface. The different binding

sites observed in the complex may thus have different preferences for Gb_3 species.

Mutagenesis studies have identified residues in each binding site that, upon mutation, cause a reduction in binding affinity. However, mutation of Trp34 to alanine does not decrease the apparent binding affinity (D. Bast and J. L. Brunton, unpublished results), although the number of molecules bound to Gb_3 in a microtiter assay is significantly reduced. This argues against an essential role for site 3 in cell binding, as Trp34 is involved in many of the interactions in this site. Interestingly, a structure of the GT3 mutant of SLT-IIe in complex with Pk-MCO only has sites 1 and 2 occupied, even though Trp34 is conserved (H. Ling and J. L. Read, unpublished results). This also suggests that site 3 has a lower affinity. However, spectroscopy indicates that Gb_3 binding alters the environment and conformation of Trp34 (*55*). Since the spectroscopy study was carried out in solution, this suggests that binding at site 3 is not just an artifact of the crystalline environment. In addition, binding is observed at site 3 in 20 crystallographically different environments since there are 20 monomers of the B subunits in the asymmetric unit.

Although the affinity of site 3 may be too low to contribute significantly to the strength of cell binding, it may serve other purposes. One reason to believe that this may be the case is the fact that a tryptophan residue is conserved at this position even though it is fully exposed to the solvent. One possibility is that Gb_3 binding at site 3 drives a conformational change of the Trp34 side chain from a disordered state (as in SHT) to an ordered 5-fold symmetric state. Such a change could potentially affect the A2 peptide, which protrudes from the pore in the B-pentamer. A more complete search for biological effects of the W34A mutant and other substitutions at this site will be required to resolve this matter.

Site 3 might also play a role by helping to sequester more Gb_3 molecules in the membrane below the toxin. Indeed, the local density of binding sites was unexpected, and it is tempting to speculate that the density of glycolipid molecules could have functional consequences, either through the high concentration of ceramide tails or through a local effect on membrane fluidity. The high local concentration of Gb_3 molecules could be involved in generating the intracellular signal that leads to apoptosis, upon binding of SLT-I B-pentamers to Burkitt's lymphoma cells (*61*). Alternatively, a cluster of Gb_3 molecules might tend to segregate in membrane bilayers of a particular thickness. This could play a role in intracellular trafficking of the toxin; different organelles have different lipid compositions, and the length of membrane-spanning helixes in membrane proteins has been shown to influence their subcellular distribution (*62*, *63*).

The crystallographic observation of the interactions of the Gb_3 trisaccharide with the SLT-I B-subunit can provide the basis for the rational development of new therapies based on sequestering the toxin or interfering with its interaction with target cells. Modifications of the natural trisaccharide can be designed to take advantage of new interactions with neighboring residues. In addition, the discovery of multiple binding sites opens new avenues, as it makes possible the design of carbohydrate analogues with higher valency. It should be possible to join two carbohydrate molecules with a linker that spans the distance between two of the observed binding sites. Improved ligands could lead to improvements in the Pk-Synsorb therapy currently under investigation (*20*, *21*).

ACKNOWLEDGMENT

We thank Dr. Norma E. C. Duke for collecting the initial diffraction data set, Dr. Marie E. Fraser for sharing Shiga toxin coordinates prior to deposition, and Dr. Pavel Kitov for sharing his insights into carbohydrate conformation. Dr. Robert Ippolito of the Alberta Research Council kindly supplied us with Pk-MCO, the Gb_3 analogue used in this study.

REFERENCES

1. Brunton, J. L. (1990) in *The Bacteria Molecular Basis of Bacterial Pathogenesis* (Iglewski, B., and Clark, V.,Eds.) Vol. 11, pp 377−398, Academic Press, New York.
2. O'Brien, A. D., Newland, J., Miller, S. F., Holmes, R. K., Smith, H. W., and Formal, S. F. (1984) *Science 226*, 694−696.
3. Marques, L. R., Moore, M. A., Wells, J. G., Wachsmuth, I. K., and O'Brien, A. D. (1986) *J. Infect. Dis. 154*, 338−341.
4. Kovacs, M. J., Roddy, J., Gregoire, S., Cameron, W., Eidus, L., and Drouin, J. (1990) *Am. J. Med. 88*, 177−179.
5. Karmali, M. A., Petric, M., Lim, C., Fleming, P. C., Arbus, G. S., and Lior, H. (1985) *J. Infect. Dis. 151*, 775−782.
6. Fong, J. S., de Chadarevian, J. P., and Kaplan, B. S. (1982) *Pediatr. Clin. North Am. 29*, 835−856.
7. Rowe, P. C., Orrbine, E., Wells, D. A., and McLaine, P. N. (1991) *J. Pediatr. 119*, 218−224.
8. Cimolai, N., Carter, J. E., Morrison, B. J., and Anderson, J. D. (1990) *J. Pediatr. 116*, 589−592.
9. Walterspiel, J. N., Ashkenazi, S., Morrow, A. L., and Cleary, T. G. (1992) *Infection 20*, 25−29.
10. Gill, D. M. (1978) in *Bacterial Toxins and Cell Membranes* (Jeljaszewica, J., and Wadstrom, T., Eds.) pp 291−332, Academic Press, New York.
11. Olsnes, S., Reisbig, R., and Eiklid, K. (1981) *J. Biol. Chem. 256*, 8732−8738.
12. Donohue-Rolfe, A., Keusch, G., Edson, C., Thorley-Lawson, D., and Jacewicz, M. (1984) *J. Exp. Med. 160*, 1767−1781.
13. Endo, Y., Tsurugi, K., Yutsudo, T., Takeda, Y., Ogasawara, K., and Igarashi, K. (1988) *Eur. J. Biochem. 171*, 45−50.
14. Fraser, M., Chernaia, M., Kozlov, Y., and James, M. N. G. (1994) *Nat. Struct. Biol. 1*, 59−64.
15. Donohue-Rolfe, A., Jacewicz, M., and Keusch, G. T. (1989) *Mol. Microbiol. 3*, 1231−1236.
16. Jacewicz, M., Clausen, H., Nudelman, E., Donohue-Rolfe, A., and Keusch, G. (1986) *J. Exp. Med. 163*, 1391−1404.
17. Lindberg, A., Brown, J. E., Strömberg, N., Westling-Ryd, M., Schultz, J. E., and Karlsson, K. (1987) *J. Biol. Chem. 262*, 1779−1785.
18. Waddell, T., Head, S., Petric, M., Cohen, A., and Lingwood, C. A. (1988) *Biochem. Biophys. Res. Commun. 152*, 674−679.
19. Weinstein, D. L., Jackson, M. P., Perera, L. P., Holmes, R. K., and O'Brien, A. D. (1989) *Infect. Immun. 57*, 3743−3750.
20. Armstrong, G. D., Fodor, E., and Vanmaele, R. (1991) *J. Infect. Dis. 164*, 1160−1167.
21. Armstrong, G. D., Rowe, P. C., Goodyer, P., Orrbine, E., Klassen, T. P., Wells, G., Mackenzie, A., Lior, H., Blanchard C., Auclair, F., Thompson, B., Rafter, D. J., and McLaine, P. N. (1995) *J. Infect. Dis. 171*, 1042−1045.
22. Strockbine, N. A., Jackson, M. P., Sung, L. M., Holmes, R. K., and O'Brien, A. D. (1988) *J. Bacteriol. 170*, 1116−1122.
23. DeGrandis, S., Ginsberg, J., Toone, M., Climie, S., Friesen, J., and Brunton, J. L. (1987) *J. Bacteriol. 169*, 4313−4319.
24. Stein, P. E., Boodhoo, A., Tyrrell, G. J., Brunton, J. L., and Read, R. J. (1992) *Nature 355*, 748−750.
25. Nyholm, P.-G., Brunton, J. L., and Lingwood, C. A. (1995) *Int. J. Biol. Macromol. 17*, 199−204.

26. Nyholm, P.-G., Magnusson, G., Zheng, Z., Norel, R., Binnington-Boyd, B., and Lingwood, C. A. (1996) *Chem. Biol. 3*, 263−275.
27. Ramotar, K., Boyd, B., Tyrrell, G. J., Gariepy, J., Lingwood, C. A., and Brunton, J. L. (1990) *Biochem. J. 272*, 805−811.
28. Howard, A. J., Gilliland, G. L., Finzel, B. C., Poulos, T. L., Ohlendorf, D. H., and Salemme, F. R. (1987) *J. Appl. Crystallogr. 20*, 383−387.
29. Navaza, J. (1987) *Acta Crystallogr. A 43*, 645−653.
30. Navaza, J. (1990) *Acta Crystallogr. A 46*, 619−620.
31. Fujinaga, M., and Read, R. J. (1987) *J. Appl. Crystallogr. 20*, 517−521.
32. Sixma, T. K., Stein, P. E., Hol, W. G. J., and Read, R. J. (1993) *Biochemistry 32*, 191−198.
33. Brünger, A. T. (1992a) *X-PLOR, version 3.1. A system for X-ray Crystallography and NMR*, Yale University Press, New Haven and London.
34. Read, R. J. (1986) *Acta Crystallogr. A 42*, 140−149.
35. Brünger A. T. (1992b) *Nature 355*, 472−475.
36. Kleywegt, G. J., and Brünger, A. T. (1996) *Structure 4*, 897−904.
37. Jones, T. A., Zou, J.-Y., Cowan, S. W., and Kjeldgaard, M. (1991) *Acta Crystallogr. A 47*, 110−119.
38. Vellieux, F. M. D. A. P., Hunt, J. F., Roy, S., and Read, R. J. (1995) *J. Appl. Crystallogr. 28*, 347−351.
39. Sim, G. A. (1959) *Acta Crystallogr. 12*, 813−815.
40. Bricogne, G. (1976) *Acta Crystallogr. A 32*, 832−847.
41. Jiang, J. S., and Brünger, A. T. (1994) *J. Mol. Biol. 243*, 100−115.
42. Murzin, A. G., (1993) *EMBO J. 12*, 861−867.
43. Merritt, E. A., Sarfaty, S., van den Akker, F., L'hoir, C., Martial, J. A., and Hol, W. G. J. (1994) *Protein Sci. 3*, 166−175.
44. Jackson, M. P., Wadolkowski, E. A., Weinstein, D. L., Holmes, R. K., and O'Brien, A. D. (1990) *J. Bacteriol. 172*, 653−658.
45. Vyas, N. K. (1991) *Curr. Opin. Struct. Biol. 1*, 732−740.
46. Rini, J. M. (1995) *Annu. Rev. Biophys. Biomol. Struct. 24*, 551−577.
47. Quiocho, F. A., Vyas, N. K., and Spurlino, J. C. (1989) *Trans. Am. Crystallogr. Assoc. 25*, 23−35.
48. Clark, C., Bast, D., Sharp, A. M., St. Hilaire, P. M., Agha, R., Stein, P. E., Toone, E. J., Read, R. J., and Brunton, J. L. (1996) *Mol. Microbiol. 19*, 891−899.
49. Richardson, J. M., Evans, P. D., Homans, S. W. and Donohue-Rolfe, A. (1997) *Nat. Struct. Biol. 4*, 190−193.
50. Tyrrell, G. J., Ramotar, K., Toye, B., Boyd, B., Lingwood, C. A., and Brunton, J. L. (1992) *Proc. Natl. Acad. Sci. U.S.A. 89*, 524−528.
51. Cummings, M. D., Ling, H., Armstrong, G. D., Brunton, J. L., and Read, R. J. (1998) *Biochemistry 37*, 1789−1799.
52. DeGrandis, S., Law, H., Brunton, J. L., Gyles, C., and Lingwood, C. A. (1989) *J. Biol. Chem. 264*, 12520−12525.
53. Jemal, C., Haddad, J. E., Begum, D., and Jackson, M. P. (1995) Analysis of Shiga toxin subunit association by using hybrid A polypeptides and site-specific mutageneis, *J. Bacteriol. 177*, 3128−3132.
54. Nyholm, P.-G., and Pascher, I. (1993) *Biochemistry 32*, 1225−1234.
55. St. Hilaire, P. M., Boyd, M. K., and Toone, E. J. (1994) *Biochemistry 33*, 14452−14463.
56. Cuatrecasas, P. (1973) *Biochemistry 12*, 3547−3557.
57. Holmgren, J., Mansson, J. E., and Svennerholm, L. (1974) *Med. Biol. 52*, 229−233.
58. Schafer, D. E., and Thakur, A. K. (1982) *Cell Biophys. 4*, 25−40.
59. Fuchs, G., Mobassaleh, M., Donohue-Rolfe, A., Montgomery, R. K., Gerard, R. J., and Keusch, G. T. (1986) *Infect. Immun. 53*, 372−377.
60. Pellizzari, A., Pang, H., and Lingwood, C. A. (1992) *Biochemistry 31*, 1363−1370.
61. Mangeney, M., Lingwood, C. A., Taga, S., Caillou, B., Tursz, T., and Wiels, J. (1993) *Cancer Res. 53*, 5314−5319.
62. Masibay, A. S., Balaji, P. V., Boeggeman, E. E., and Qasba, P. K. (1993) *J. Biol. Chem. 268*, 9908−9916.
63. Bretscher, M. S., and Munro, S. (1993) *Science 261*, 1280−1281.
64. Laskowski, R. A., MacArthur, M. W., Moss, D. S., and Thornton, J. M. (1993) *J. Appl. Crystallogr. 26*, 283−291.
65. Kraulis, P. J. (1991) *J. Appl. Crystallogr. 24*, 946−950.
66. Esnouf, R. M. (1997) *J. Mol. Graphics 15*, 133−138.
67. Nicholls, A., Sharp, K. A., and Honing, B. (1991) *Proteins 11*, 281−296.

BI971806N